ICIC Express Letters
Part B: Applications
Volume **8**, Number **6**, June **2017**

ICIC International ©2017 ISSN 2185-2766
pp. 945–954

AN ADAPTIVE HYBRID FILTER FOR INERTIAL/MAGNETIC HUMAN-MOTION-CAPTURE SYSTEM

Yongle Lu, Shuang Gong, Ke Di, Yan Wang, Xin Zhang and Yu Liu*

Chongqing Municipal Level Key Laboratory of Photoelectronic Information Sensing
and Transmitting Technology
Chongqing University of Posts and Telecommunications
No. 2, Chongwen Road, Nan'an District, Chongqing 400065, P. R. China
*Corresponding author: xouxousun@163.com

Received December 2016; accepted March 2017

Abstract. *An analytically derived method with generated information is designed for dealing with the high-frequency noises and gyro drift of the Human-Motion-Capture System with inertial and magnetic sensors, which is referred to as adaptive hybrid filter in this paper. To approach the challenges of accuracy and real time performance in Human-Motion-Capture System, we propose a novel scheme based on the Gauss-Newton Algorithm and complementary filter. We use a simplified Gauss-Newton Algorithm to process the accelerometer and magnetic data, which has the advantage of only one iteration calculation to reduce the computation complexity. The sensor fusions between attitude angles from simplified Gauss-Newton Algorithm and gyroscope data are performed using the complementary filter. Moreover, for promoting adaptability, the gravity vector and the geomagnetic reference vector are introduced to modify the parameter adaptively. We have evaluated the proposed scheme in sudden acceleration and magnetic field environments. The experimental results have demonstrated that the mean error was 0.94° in magnetic interference state and the mean error was lower than 1° in dynamic environment. Moreover, the algorithm execution time has been reduced by 25% compared with Extended Kalman Filter, and it has achieved the accurate reproduction of the system.*
Keywords: Inertial sensors, Attitude estimation, Gauss-Newton Algorithm, Complementary filter, Human-Motion-Capture System

1. **Introduction.** Recent years have witnessed the rapid development and intensive study of the Human-Motion-Capture System (HMCS). The new technology is widely applied into effects-driven films, human rehabilitation exercises and other sences. Because of the high price and limited application scenarios of the matured HMCS based on optical instruments [1], it has difficulties in popularized engineering and business applications. So most of the current work has focused on the application of Micro-Electro-Mechanical System (MEMS) inertial sensors in HMCS. However, the low-frequency drifts of gyroscope and high-frequency noises of magnetometer affect the final outputs [2]. Therefore, we can fuse the data by using a stochastic approach and a frequency analysis.

Among the stochastic approaches, sensor fusion methods for orientation estimation determination can be designed using approaches based either on Kalman Filter (KF) or nonlinear complementary filter. KF is a recursive filter based on time-varying linear system [3]. Extended Kalman Filter (EKF) is strict to linear error, local truncation error and filter divergence [4,5]. Linear Kalman filter can reduce the effect of high frequency interference on accelerometer and magnetometer [6]. Anti-jamming algorithm based on Unscented Kalman Filter (UKF) avoids the disadvantage of white noise on attitude resolution [7]. In different application scenarios, KF needs harsh conditions; besides, we need to establish the appropriate state equations, process equations under different conditions, requiring a large number of arithmetic operations [8]. A new algorithm of attitude data

fusion, based on complementary filtering and conjugate gradient-descent method, is used to improve the convergence speed of the algorithm [9]. Hybrid Filter (HF) combines with the principle of the gradient descent method and the complementary filtering algorithm [10], but the adaptability and accuracy are restricted by the quantitative parameter of complementary filtering.

We propose an Adaptive Hybrid Filter (AHF) based on simplified Gauss-Newton Algorithm (SGNA) and complementary filter to overcome the above challenges. The overall program is illustrated in Figure 1. Magnetometer data and accelerometer data are processed by SGNA. A complementary filter is used to fuse the sensor data, avoiding the interference high frequency noise and gyro drift. In order to raise the dynamic performance of filter, we use the gravity vector, reference geomagnetic vector to adjust the parameters of the complementary filter. Moreover, the convergence direction of the SGNA is used as the observation vector to compensate the gyroscope drift error.

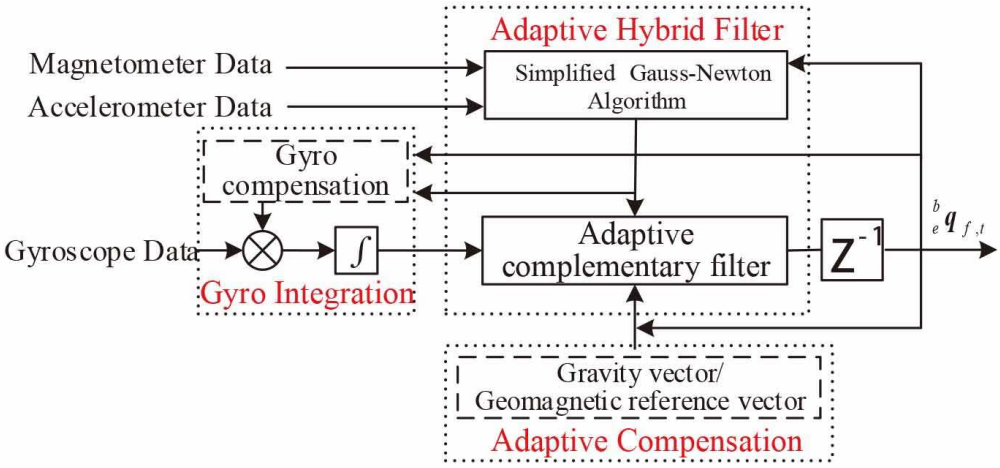

FIGURE 1. Framework of the proposed algorithm

The rest of paper is organized as follows. Section 1 introduces the algorithm framework. Section 2 and Section 3 discuss the SGNA and AHF according to the dataflow. Section 4 shows the experimental validation and results. Finally, conclusions are given in Section 5.

2. Simplified Gauss-Newton Algorithm.

2.1. Attitude described by quaternion.

The three-axis angular rate data of the gyroscope are converted to the form of quaternion, shown as Equation (1). The quaternion derivation ${}^b_e\dot{\mathbf{q}}_\omega$ describing the rate of change of orientation in the sensor frame relative to the earth frame can be calculated as Equation (2).

$$ {}^b\omega = \begin{bmatrix} 0 & \omega_x & \omega_y & \omega_z \end{bmatrix} \tag{1} $$

$$ {}^b_e\dot{\mathbf{q}}_\omega = \frac{1}{2} {}^b_e\hat{\mathbf{q}} \otimes {}^b\omega \tag{2} $$

where the left superscript b and subscript e of $\dot{\mathbf{q}}_\omega$ imply that the corresponding vectors are expressed in the sensor and earth frame coordinates, respectively, and ${}^b_e\hat{\mathbf{q}}$ is the rotation matrix of the sensor frame with respect to the earth frame, and ${}^b\omega$ is the angular velocity.

In accordance with the properties of quaternion, the attitude quaternion ${}^b_e\mathbf{q}_{\omega,t+\Delta t}$ and its derivative ${}^b_e\dot{\mathbf{q}}_{\omega,t+\Delta t}$ at time $t+\Delta t$ can be calculated iteratively by Equation (3) and Equation (4):

$$ {}^b_e\mathbf{q}_{\omega,t+\Delta t} = {}^b_e\hat{\mathbf{q}}_{\omega,t} + {}^b_e\dot{\mathbf{q}}_{\omega,t+\Delta t}\Delta t \tag{3} $$

$$ {}^{b}_{e}\dot{\mathbf{q}}_{\omega,t+\Delta t} = \frac{1}{2} {}^{b}_{e}\hat{\mathbf{q}}_{\omega,t} \otimes {}^{b}\omega_{t+\Delta t} \tag{4} $$

where Δt is the sampling period. We can update the attitude by the three-axis angular velocity of the gyroscope, Equation (3) and Equation (4).

2.2. **Simplified Gauss-Newton Algorithm.** We estimate the orientation using Gauss-Newton Algorithm by the difference between the converted value and measured value. We can get the objective function by the nonlinear least mean square error.

$$ f\left({}^{b}_{e}\hat{\mathbf{q}}_{am,t}\right) = \frac{1}{2}\varepsilon\left({}^{b}_{e}\hat{\mathbf{q}}_{am,t}\right)^{T}\varepsilon\left({}^{b}_{e}\hat{\mathbf{q}}_{am,t}\right) \tag{5} $$

where ${}^{b}_{e}\hat{\mathbf{q}}_{am,t}$ is quaternion calculated with Gauss-Newton iterative algorithm, and $\varepsilon\left({}^{b}_{e}\hat{\mathbf{q}}_{am,t}\right)$ is the error function.

The gravity vector and the geomagnetic reference vector are ${}^{e}\hat{\mathbf{z}}_{a,t} = \begin{bmatrix} 0 & 0 & 0 & 1 \end{bmatrix}$ and ${}^{e}\hat{\mathbf{z}}_{m,t} = \begin{bmatrix} 0 & \hat{m}_x & \hat{m}_y & \hat{m}_z \end{bmatrix}$, respectively. According to the characteristics of the quaternion, we can get Equation (6) and Equation (7):

$$ {}^{b}_{e}\hat{\mathbf{Q}}_{a,t} = {}^{b}_{e}\hat{\mathbf{q}}_{am,t} \otimes {}^{e}\hat{\mathbf{z}}_{a,t} \otimes {}^{b}_{e}\hat{\mathbf{q}}^{*}_{am,t} \tag{6} $$

$$ {}^{b}_{e}\hat{\mathbf{Q}}_{m,t} = {}^{b}_{e}\hat{\mathbf{q}}_{am,t} \otimes {}^{e}\hat{\mathbf{z}}_{m,t} \otimes {}^{b}_{e}\hat{\mathbf{q}}^{*}_{am,t} \tag{7} $$

${}^{b}\hat{\mathbf{a}}_t$ and ${}^{b}\hat{\mathbf{m}}_t$ stand for the normalized vector of the triaxial data of accelerometer and magnetometer, respectively. We get the error function by the weight of the accelerometer ρ_a and the weight of the magnetometer ρ_m:

$$ \varepsilon\left({}^{b}_{e}\hat{\mathbf{q}}_{am,t}\right) = \begin{bmatrix} \rho_a\varepsilon_a\left({}^{b}_{e}\hat{\mathbf{q}}_{am,t}\right) \\ \rho_m\varepsilon_m\left({}^{b}_{e}\hat{\mathbf{q}}_{am,t}\right) \end{bmatrix} = \begin{bmatrix} \rho_a\left({}^{b}_{e}\hat{\mathbf{Q}}_{a,t} - {}^{b}\hat{\mathbf{a}}_t\right) \\ \rho_m\left({}^{b}_{e}\hat{\mathbf{Q}}_{m,t} - {}^{b}\hat{\mathbf{m}}_t\right) \end{bmatrix} \tag{8} $$

where ${}^{b}\mathbf{a}$ and ${}^{b}\mathbf{m}$ are the external acceleration and magnetic field.

We can get the result of equation according to the definition of matrix two-norm when $\left\|\varepsilon\left({}^{b}_{e}\hat{\mathbf{q}}_{am,t}\right)\right\| = 0$. Iterative formula can be calculated by using Gauss-Newton iterative algorithm, which is expressed as:

$$ {}^{b}_{e}\hat{\mathbf{q}}(k+1) = {}^{b}_{e}\hat{\mathbf{q}}(k) - \left(J(k)^{T}J(k)\right)^{-1}J(k)^{T}\varepsilon\left({}^{b}_{e}\hat{\mathbf{q}}(k)\right) \quad (k = 0, 1, 2, \ldots, n) \tag{9} $$

$\mathbf{J}(k)$ is the Jacobian determinant of error equation in the current moment:

$$ \mathbf{J}\left({}^{b}_{e}\hat{\mathbf{q}}(k)\right) = \frac{\partial\varepsilon\left({}^{b}_{e}\hat{\mathbf{q}}(k)\right)}{\partial {}^{b}_{e}\hat{\mathbf{q}}(k)} = \begin{bmatrix} \rho_a\dfrac{\partial\varepsilon_1}{\partial\hat{q}_0} & \rho_a\dfrac{\partial\varepsilon_1}{\partial\hat{q}_x} & \rho_a\dfrac{\partial\varepsilon_1}{\partial\hat{q}_y} & \rho_a\dfrac{\partial\varepsilon_1}{\partial\hat{q}_z} \\ \vdots & \vdots & \vdots & \vdots \\ \rho_m\dfrac{\partial\varepsilon_6}{\partial\hat{q}_0} & \rho_m\dfrac{\partial\varepsilon_6}{\partial\hat{q}_x} & \rho_m\dfrac{\partial\varepsilon_6}{\partial\hat{q}_y} & \rho_m\dfrac{\partial\varepsilon_6}{\partial\hat{q}_z} \end{bmatrix} \tag{10} $$

Equation (11) describes the traditional Gauss-Newton Algorithm to estimate attitude using the initial value.

$$ \begin{aligned} {}^{b}_{e}\hat{\mathbf{q}}(n+1) &= {}^{b}_{e}\hat{\mathbf{q}}(0) - \sum_{k=0}^{n}\left(\mathbf{J}(k)^{T}\mathbf{J}(k)\right)^{-1}\mathbf{J}(k)^{T}\varepsilon\left({}^{b}_{e}\hat{\mathbf{q}}(k)\right) \\ &= {}^{b}_{e}\hat{\mathbf{q}}(0) - \mu_k\left(\mathbf{J}(0)^{T}\mathbf{J}(0)\right)^{-1}\mathbf{J}(0)^{T}\varepsilon\left({}^{b}_{e}\hat{\mathbf{q}}(0)\right) \end{aligned} \tag{11} $$

where ${}^{b}_{e}\hat{\mathbf{q}}(n+1)$ is the rotation quaternion calculated with the Gauss-Newton Algorithm at $t+\Delta t$, recorded as ${}^{b}_{e}\hat{\mathbf{q}}_{am,t+\Delta t}$. ${}^{b}_{e}\hat{\mathbf{q}}(0)$ is the initial attitude calculated with complementary filtering algorithm at t, recorded as ${}^{b}_{e}\hat{\mathbf{q}}_{f,t}$. μ_t is the step-size, which can be calculated with Hessen matrix of objective function. Ignoring the two-order information item of Hessen matrix, we get the faster convergence speed based on approximate term $H \approx 2\mathbf{J}^{T}\mathbf{J}$ and gradient $\mathbf{G} \approx 2\mathbf{J}^{T}\varepsilon$, recorded as $\nabla = -\left(\mathbf{J}^{T}\mathbf{J}\right)^{-1}\mathbf{J}^{T}\varepsilon$.

The iteration times of Gauss-Newton Algorithm are constrained by the convergence rate. The convergence speed is no less than the carrier, while constrained by the step-size. The iterative time can be shortened by giving the step-size μ_t an appropriate value. Thus, Equation (11) can be simplified as follows:

$$\begin{aligned} {}^b_e\hat{\mathbf{q}}_{am,t+\Delta t} &= {}^b_e\hat{\mathbf{q}}_{f,t} - \mu_{t+\Delta t}\left(\mathbf{J}\left({}^b_e\hat{\mathbf{q}}_{f,t}\right)^T J\left({}^b_e\hat{\mathbf{q}}_{f,t}\right)\right)^{-1} J\left({}^b_e\hat{\mathbf{q}}_{f,t}\right)^T \varepsilon\left({}^b_e\hat{\mathbf{q}}_{f,t}\right) \\ &= {}^b_e\hat{\mathbf{q}}_{f,t} - \mu_{t+\Delta t}\frac{\nabla^b_e\hat{\mathbf{q}}_{f,t}}{\|\nabla^b_e\hat{\mathbf{q}}_{f,t}\|} \end{aligned} \tag{12}$$

The optimal value of the step-size $\mu_{t+\Delta t}$ can be calculated as Equation (13) [11].

$$\mu_{t+\Delta t} = \alpha \left\|{}^b_e\dot{\mathbf{q}}_{\omega,t+\Delta t}\right\| \Delta t \tag{13}$$

The attitude quaternion ${}^b_e\hat{\mathbf{q}}_{am,t+\Delta t}$ can be calculated iteratively by Equation (12). With the improvement of our work, only one iteration is required for each solution, which greatly reduces the computational complexity.

3. **Adaptive Hybrid Filtering Algorithm.** Two different solutions of attitude angles are discussed separately in Section 2. However, the accuracy of the solution will be decreased for the drifts of gyroscope measuring data, affected by low frequency noise. Besides, it is difficult to converge to the optimal value using SGNA under high frequency noise and the linear acceleration interference.

3.1. **Estimation of orientation based on adaptive hybrid algorithm.** The complementary filter can be used to process the two noise sources. The high-pass filter processes the gyroscope data, and the low-pass filter deals with the data of the other two sensors. The final optimal attitude angle is fused by ${}^b_e\hat{\mathbf{q}}_{\omega,t}$, integrated over gyroscope data and ${}^b_e\hat{\mathbf{q}}_{am,t}$, solved by SGNA. In this paper, the adaptive complementary filter combines the advantages of both the complementary filter and SGNA. The proposed method adjusts the factors in real-time system to improve the accuracy.

The fusion formula for the basic complementary filtering algorithm is calculated from Equation (14):

$${}^b_e\hat{\mathbf{q}}_{f,t} = k_t {}^b_e\hat{\mathbf{q}}_{a,t} + (1-k_t){}^b_e\hat{\mathbf{q}}_{\omega,t}, \quad 0 \le k_t \le 1 \tag{14}$$

where k_t and $1-k_t$ are the weights of the two kinds of attitude solving schemes. The value of k_t, which guarantees the covergence rate of ${}^b_e\hat{\mathbf{q}}_{am,t}$, is restricted to the physical orientation rate measured from gyroscope ${}^b_e\hat{\mathbf{q}}_{\omega,t}$. Therefore, the value of k_t can be calculated as (15).

$$k_t\frac{\mu_t}{\Delta t} = \lambda\left(1-k_t\right), \text{ namely, } k_t = \frac{\lambda}{\mu_t/\Delta t + \lambda} \tag{15}$$

where λ is the variable parameter after simplifying. Substituting Equation (13) and Equation (15) into Equation (14) obtains Equation (16).

$${}^b_e\hat{\mathbf{q}}_{f,t} = \frac{\lambda}{\alpha\left\|{}^b_e\dot{\mathbf{q}}_{\omega,t+\Delta t}\right\| + \lambda}{}^b_e\hat{\mathbf{q}}_{am,t} + \left(\frac{\alpha\left\|{}^b_e\dot{\mathbf{q}}_{\omega,t+\Delta t}\right\|}{\alpha\left\|{}^b_e\dot{\mathbf{q}}_{\omega,t+\Delta t}\right\| + \lambda}\right){}^b_e\hat{\mathbf{q}}_{\omega,t} \tag{16}$$

Equation (16) contains two parameters α and λ. Considering that the convergence rate of ${}^b_e\hat{\mathbf{q}}_{am,t}$ cannot be less than the actual velocity of the movement of the carrier, Equation (12) and Equation (15) can be written as follows.

$${}^b_e\dot{\mathbf{q}}_{am,t+\Delta t} = -\mu_{t+\Delta t}\frac{\nabla^b_e\hat{\mathbf{q}}_{f,t}}{\|\nabla^b_e\hat{\mathbf{q}}_{f,t}\|} \tag{17}$$

$$k_t = \frac{\lambda}{\mu_t/\Delta t} = \frac{\lambda\Delta t}{\mu_t} \tag{18}$$

Since μ_t is large, we can get that $k_t \approx 0$. Substituting Equation (3), Equation (17) and Equation (18) into Equation (14) obtains Equation (19).

$$ {}^{b}_{e}\hat{\mathbf{q}}_{f,t+\Delta t} = {}^{b}_{e}\hat{\mathbf{q}}_{f,t} + {}^{b}_{e}\dot{\mathbf{q}}_{f,t+\Delta t}\Delta t \tag{19} $$

where

$$ {}^{b}_{e}\dot{\mathbf{q}}_{f,t+\Delta t} = {}^{b}_{e}\dot{\mathbf{q}}_{\omega,t+\Delta t} - \lambda {}^{b}_{e}\dot{\mathbf{q}}_{\nabla,t+\Delta t} = {}^{b}_{e}\dot{\mathbf{q}}_{\omega,t+\Delta t} - \lambda \frac{\nabla {}^{b}_{e}\hat{\mathbf{q}}_{f,t}}{\|\nabla {}^{b}_{e}\hat{\mathbf{q}}_{f,t}\|} \tag{20} $$

λ is the only one parameter of the simplified complementary filter fusion algorithm. The optimized λ is as follows:

$$ \lambda = 2 - (e_{a,t} + e_{m,t}) * 0.9 - (|e_{ax}| + |e_{ay}| + |e_{az}| + |e_{mx}| + |e_{my}| + |e_{mz}|) * 10 * 0.1 \tag{21} $$

where $e_{a,t}$ and $e_{m,t}$ are the previous error vectors of accelerometer and magnetometer, respectively. The calculation method of the errors is as follows:

$$ \mathbf{e}_a = \begin{bmatrix} e_{a0} & e_{ax} & e_{ay} & e_{az} \end{bmatrix}^{\mathrm{T}} = {}^{e}\hat{\mathbf{z}}_{a,t} \otimes {}^{b}\hat{\mathbf{a}} \tag{22} $$

$$ \mathbf{e}_m = \begin{bmatrix} e_{m0} & e_{mx} & e_{my} & e_{mz} \end{bmatrix}^{\mathrm{T}} = {}^{b}\hat{\mathbf{m}} \otimes {}^{e}\hat{\mathbf{z}}_{m,t} \tag{23} $$

The optimized formula reduces the changing rate of adaptive filtering parameters and improves continuity and stability of the system, which incorporates low-pass filter.

3.2. **Gyroscope drift compensation.** In order to reduce the effect of gyroscope drift on the measurement accuracy, the convergence direction of the SGNA algorithm is used as the observation vector to compensate the gyroscope drift error. The angular velocity after compensation is as follows:

$$ {}^{b}\omega_{c,t+\Delta t} = {}^{b}\omega_{t+\Delta t} - {}^{b}\omega_{error,t+\Delta t} \tag{24} $$

where

$$ {}^{b}\omega_{error,t+\Delta t} = 2 {}^{b}_{e}\hat{\mathbf{q}}^{*}_{f,t+\Delta t} \otimes {}^{b}_{e}\dot{\mathbf{q}}_{\nabla,t+\Delta t} \tag{25} $$

The schematic diagram of the improved adaptive complementary filtering algorithm is shown in Figure 2.

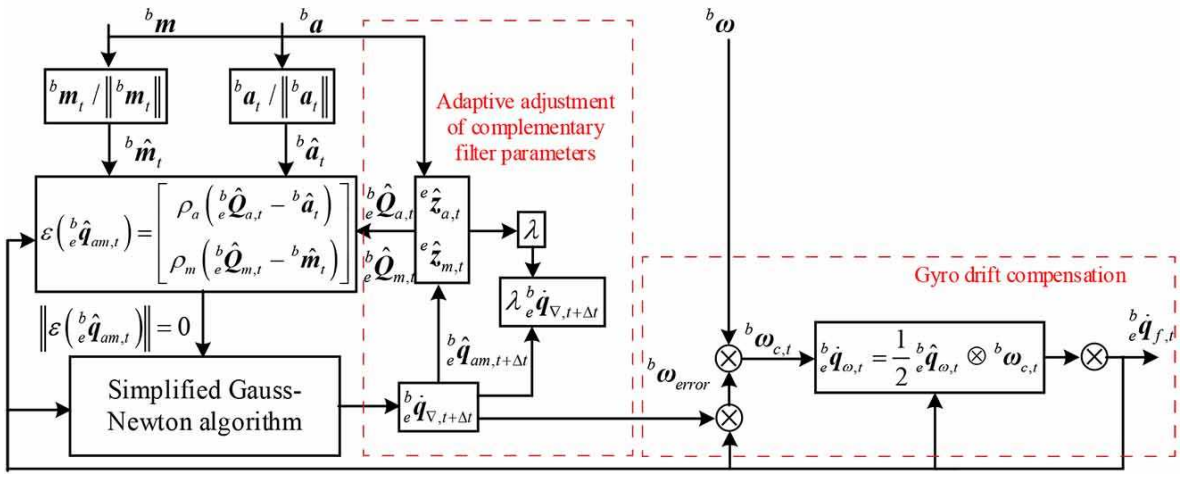

FIGURE 2. Schematic diagram of AHF

4. **Experimental Validation and Results.** Figure 3 shows the inertial/magnetic sensor, including a gyroscope and an accelerometer, integrated in a chip named MPU6050 and a tri-axis magnetometer (HMC5883). The small chip is based on the Wireless bluetooth communication, and the sampling frequency of 100Hz is supposed to work well for HMCS.

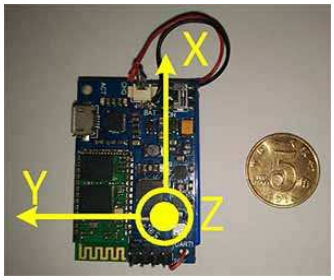

FIGURE 3. Inertial/magnetic sensor

FIGURE 4. Source of disturbance in magnetic

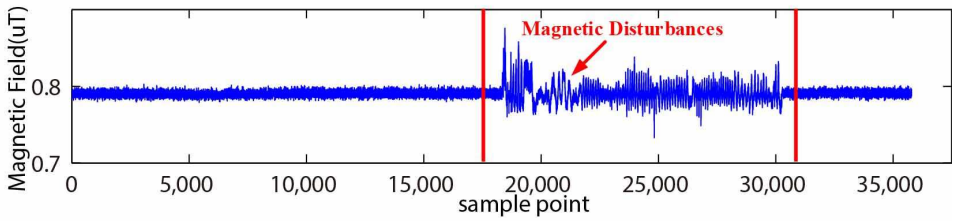

FIGURE 5. Modulus of the three axis magnetometer

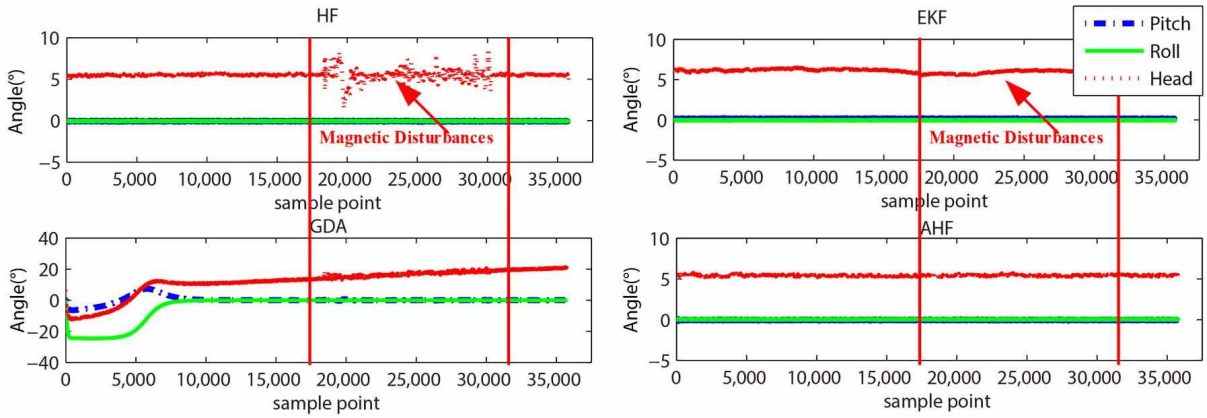

FIGURE 6. Static orientation estimation with magnetic disturbances using the proposed AHF compared with the HF, EKF, and GDA

4.1. **No movement with magnetic disturbances.** In this test scenario, the sensor arrays kept still and a magnetic was swayed around the sensor intermittently (see Figure 4). Magnetic field intensity was clearly shown in Figure 5, and the magnetic disturbances were marked in the red flags.

Figure 6 shows the Euler angles which were calculated from the HF, EKF, Gradient Descent Algorithm (GDA), and the proposed algorithm AHF. Obviously, the heading angles were evidently affected by the magnetic disturbances using the HF, and GDA, while there was no obvious influence based on the EKF and AHF. Besides, for the static accuracy, the convergence velocity of GDA is slower than all other three methods. Moreover, the proposed AHF has lower error average in static without magnetic disturbances, whose mean error is 0.5 degree.

The magnetic data are mainly involved in the calculation of the heading angle, so the effect of the magnetic disturbance on the attitude calculation has been researched. The calculation error of head angle of each algorithm is shown in Figure 7. The calculation shows that the errors of HF and GDA are 3.53° and 7.81° caused by magnetic disturbance. The values are clearly higher than the errors of EKF and AHF, which are 1.07°

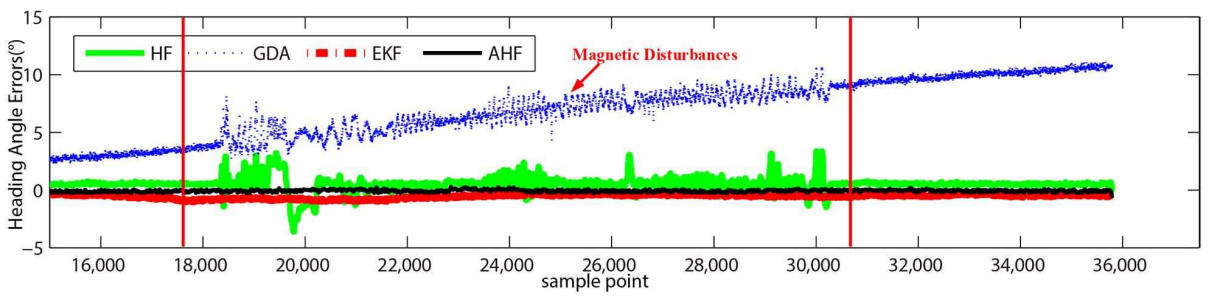

FIGURE 7. Errors of yaw with magnetic disturbances using the proposed AHF compared with the HF, EKF, and GDA

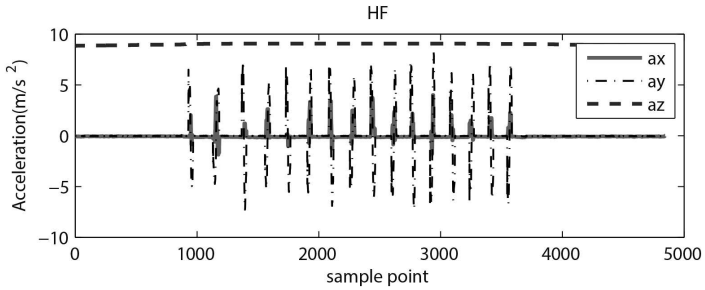

FIGURE 8. Measured data of the three axis accelerometer

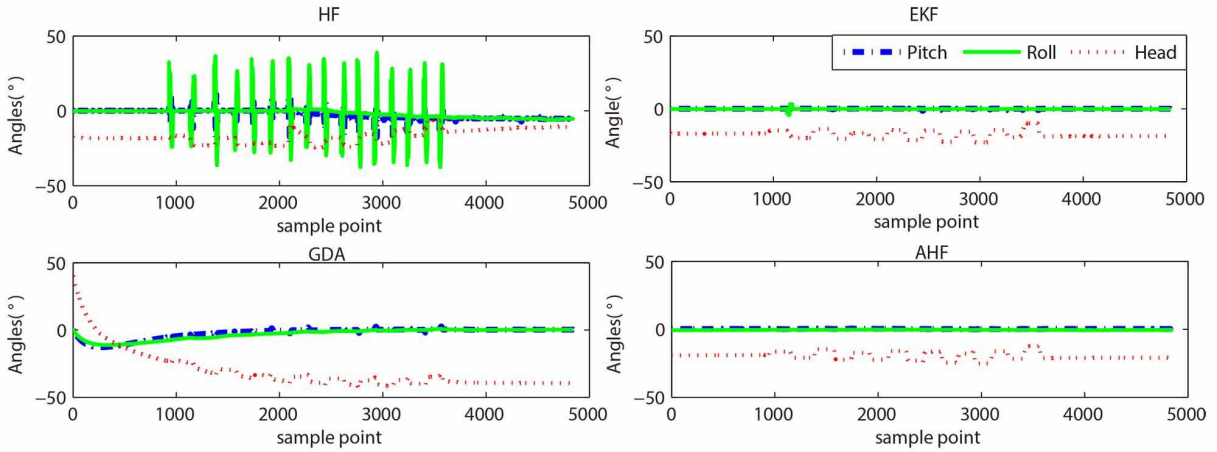

FIGURE 9. Orientation estimation with sudden fast movement using the proposed AHF compared with the HF, EKF, and GDA

and 0.94°. EKF and the proposed algorithm can effectively reduce the impact of magnetic interference on the course, which can meet the accuracy of angle with magnetic disturbance.

4.2. **Sudden fast movement.** This test was performed in a magnetically homogeneous environment and the sensor went through a sudden acceleration change. The sudden acceleration disturbances for three axes were clearly shown in Figure 8.

As shown in Figure 9, the proposed algorithm shows better performance than others in sudden acceleration change. The maximal errors of pitch angle and roll angle calculated by the proposed AHF were 0.82° and 0.92° respectively, since the others were 22.95° and 15.63°, 4.94° and 2.26°, 9.92° and 10.21°, separately calculated by HF, EKF and GDA. Thus, the proposed AHF offered reasonably accurate estimation performance even in this situation.

Table 1 shows the analysis results under static and dynamic environment from four methods. As shown in Figures 5-9 and Table 1, the error of attitude angle of the proposed was lower than 0.5° under the static state without magnetic interference, eliminating the drift effectively. It is obvious that there was no definite affect for head angle based on the proposed AHF, whose mean error was lower than 0.94°. Besides, the mean error was limited in 1° under the living environment from the proposed, which ensures the accuracy for Human-Motion-Capture System.

Table 1. Sample data

Methods	Errors (°)	Static/Nonmagnetic			Static/Magnetic			Dynamic		
		Roll	Pitch	Head	Roll	Pitch	Head	Roll	Pitch	Head
HF	max	1.23	1.96	3.13	1.48	3.12	5.61	15.63	22.95	19.05
	mean	0.75	0.89	1.43	1.52	1.47	3.53	13.91	18.87	15.11
EKF	max	0.56	0.42	0.84	0.63	0.45	1.51	2.26	4.94	2.15
	mean	0.20	0.25	0.56	0.31	0.27	1.07	1.86	3.54	0.91
GDA	max	7.72	7.91	8.68	8.15	7.48	10.22	10.21	9.92	15.92
	mean	4.52	5.50	6.11	6.43	6.76	7.81	7.78	8.57	10.43
AHF	max	0.41	0.52	0.91	0.58	0.62	1.04	0.92	0.82	0.98
	mean	0.23	0.26	0.48	0.27	0.29	0.94	0.65	0.69	0.85

The time of once iteration of four methods is recorded in Table 2, where the one iteration time of the proposed was 4.7ms, which could increase by 25%, and 55% compared with EKF and GDA. The proposed reduces the iteration time obviously.

Table 2. Time of one iteration of each algorithm

	HF	EKF	GDA	AHF
Running time (ms)	3.2	6.3	10.4	4.7

As shown in Table 3, due to its high computational efficiency and accuracy, the proposed AHF can be potentially implemented in a network of miniature MARG sensors for Human-Motion-Capture System.

Table 3. Comprehensive performance contrast of each algorithm

	AHF	HF	EKF	GDA
Gyro drift compensation	√	√	√	×
Magnetic disturbances	√	×	√	×
Sudden fast movement	√	×	×	√
Real-time	√	√	×	×

4.3. **Realization of upper brachial.** The Human-Motion-Capture System controls the human skeleton model, and reproduces human posture according to the features of human articular movement, which collects articular movement data on the basis of rigid body dynamics through a sensor network. Based on the above analyses, we designed a skeletal motion model consistent with human motion by loading a human skeleton file based on Microsoft Visual Studio 2010 platform and OpenGL development library environment, to achieve the capture of human brachial.

With the brachial motion process taken as an example, two sensors were mounted over the upper brachial and the lower brachial individually (see Figure 10). The wearer swung the brachial, and the system can accurately track the motion trajectories of the brachial

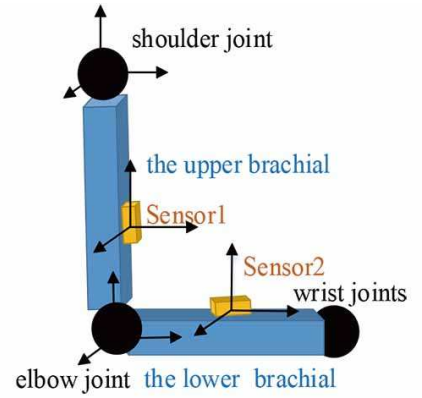

FIGURE 10. The sensors binding mode

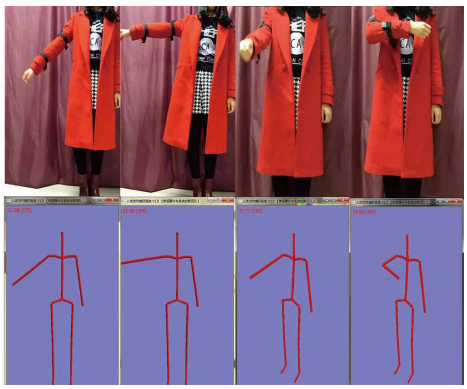

FIGURE 11. The human motion capture

(see Figure 11). With a variety of tests, the proposed AHF can accurately track the motion of the human body through the dynamic tracking of actual human bodies.

5. **Conclusions.** This paper presented an AHF with adaptive parameters designed for HMCS in free-living environments. This paper focused on adjusting the parameters of the complementary filter in real time to improve accuracy and adaptability. The proposed algorithm was evaluated under various conditions, and the results demonstrated that the mean error is 0.94° in magnetic interference state and the mean error is lower than 1° in dynamic environment. Since the proposed method needs less computation time, it is practical for HMCS.

Research is presently under-way to incorporate the AHF into the independent HMCS. Real-time performance, wireless transmission, data reliability, low power consumption, and a novel method for parametrized mannequin modelling are the major challenges in future work.

Acknowledgment. We would like to thank all the anonymous reviewers for their comments. This work was funded in part by the International Joint Research Center Technology Platform and Base Construction (cstc2014gjhz0038), Chongqing Research Program of Foundation and Advanced (cstc2015jcyjBX0068), the Doctoral Scientific Research Foundation of Chongqing University of Posts and Telecommunications (A2015-40, A2016-72, A2016-76), the National Natural Science Foundation of Chongqing Univ. of Posts and Telecommunications (A2015-49), Special Project on Transformation of Excellent Achievements in Universities of Chongqing (KJZH17115), and a grant from the intellectual property of Chongqing (CQIPO2016014).

REFERENCES

[1] P. Chen, J. Li and M. Luo, Real-time human motion capture driven by a wireless sensor network, *International Journal of Computer Games Technology*, vol.2015, no.4, pp.1-14, 2015.

[2] M. Carmona, O. Michel and J. L. Lacoume, An analytical solution for the complete sensor network attitude estimation problem, *Signal Processing*, vol.93, no.4, pp.652-660, 2013.

[3] G. Ligorio and A. M. Sabatini, A novel Kalman filter for human motion tracking with an inertial-based dynamic inclinometer, *IEEE Trans. Biomedical Engineering*, vol.62, no.8, pp.2033-2043, 2015.

[4] A. Assa and F. Janabi-Sharifi, A Kalman filter-based framework for enhanced sensor fusion, *IEEE Sensors Journal*, vol.15, no.6, pp.3281-3292, 2015.

[5] J. K. Lee, E. J. Park and S. N. Robinovitch, Estimation of attitude and external acceleration using inertial sensor measurement during various dynamic conditions, *IEEE Trans. Instrumentation and Measurement*, vol.61, no.8, pp.2262-2273, 2012.

[6] R. G. Valenti, I. Dryanovski and J. Xiao, A linear Kalman filter for MARG orientation estimation using the Algebraic quaternion algorithm, *IEEE Trans. Instrumentation and Measurement*, vol.65, no.2, pp.467-481, 2016.

[7] Z. Jiang, Y. He and J. Han, Disturbance estimation for RUAV using UKF with acceleration measurement, *IEEE International Conference on Mechatronics and Automation (ICMA)*, Beijing, China, pp.500-505, 2015.

[8] L. Zhang, Z. Xiong, J. Lai and J. Liu, Optical flow-aided navigation for UAV: A novel information fusion of integrated MEMS navigation system, *Optik – International Journal for Light and Electron Optics*, vol.127, no.1, pp.447-451, 2016.

[9] M. Euston, P. Coote and R. Mahony, A complementary filter for attitude estimation of a fixed-wing UAV, *IEEE/RSJ International Conference on Intelligent Robots and Systems*, Nice, France, pp.340-345, 2008.

[10] J. Sun, Y. You and F. Zhong, Attitude estimation based on conjugate gradient and complementary filter, *Chinese Journal of Sensors and Actuators*, vol.27, no.4, pp.524-528, 2014.

[11] S. O. Madgwick, A. J. Harrison and R. Vaidyanathan, Estimation of IMU and MARG orientation using a gradient descent algorithm, *IEEE International Conference on Rehabilitation Robotics*, Zurich, Switzerland, pp.1-7, 2011.